LASER & PHOTONICS REVIEWS

www.lpr-journal.org

Structured Vector Field Manipulation of Terahertz Wave along the Propagation Direction Based on Dielectric Metasurfaces

Jie Li, Jitao Li, Zhen Yue, Chenglong Zheng, Guocui Wang, Jingyu Liu, Hang Xu, Chunyu Song, Fan Yang, Hui Li, Fuyu Li, Tingting Tang, Yating Zhang, Yan Zhang,* and Jianquan Yao**

The generation and manipulation of vector light fields are of great significance for both fundamental research and industrial applications of polarized optics. In recent years, the spatial domain control of structured vector fields has gradually expanded from two- to three-dimensional, including traditional optics and meta-optics. Here, a new method to generate and manipulate structured vector light fields along the propagation direction is proposed, and the functionality in terahertz band using all-silicon metasurfaces is demonstrated. The coherent superposition of orthogonal circularly polarized terahertz waves through long focal depth and multifocal metalens is completed, and varying phase differences between them in the propagation direction via path accumulation or initial phase design are introduced, thereby continuous variation or independently designed vector polarization distributions in multiple planes are obtained. It is worth mentioning that the proposed scheme is not only for the design of transverse electric field components, but also shows a strong ability for manipulation of the longitudinal component. This scheme realizes the polarization distribution designs of three-dimensional vector fields in three-dimensional space, and provides a new inspiration for the generation and manipulation of vector beams based on meta-optics.

1. Introduction

Like phase, frequency, and amplitude, polarization is one of the most important parameters of electromagnetic waves, it is also a representative basis for proving that free space electromagnetic waves are transverse waves. It plays an irreplaceable role in the basic research and application fields of electromagnetism and optics. For example, circular polarization means the spin angular momentum (SAM) of photons,[1] which establishes a bridge between classical optics and quantum optics,[2] and is an important research object in chiral optics,[3,4] spin photonics,[5–7] and topological photonics.[8–10] The polarization of light has derived many new technologies in the fields of optical fiber communication,[11] 3D display,[12] remote sensing imaging,[13] etc., and promoted the technological progress of optics and photonics. Electromagnetic fields with uniform polarization distribution can be considered as scalar fields from the perspective of polarization, the main types are linear, circular, and elliptical polarizations.[14] Light beams with non-uniform polarization distributions are called vector fields, such as cylindrically symmetric vector beam.[15]

In conventional polarized optics, devices made of optical crystals like polarizers and wave plates are usually used to perform

J. Li, J. Li, Z. Yue, C. Zheng, H. Xu, C. Song, F. Yang, H. Li, Y. Zhang, J. Yao
School of Precision Instruments and Opto-Electronics Engineering
Tianjin University
Tianjin 300072, China
E-mail: yating@tju.edu.cn; jqyao@tju.edu.cn

G. Wang, J. Liu, Y. Zhang
Department of Physics
Capital Normal University
Beijing 100048, China
E-mail: yzhang@mail.cnu.edu.cn

G. Wang
School of Optics and Photonics
Beijing Institute of Technology
Beijing 100081, China

F. Li, T. Tang
Information Materials and Device Applications Key Laboratory of Sichuan Provincial, Universities
Chengdu University of Information Technology
Chengdu 610225, China

The ORCID identification number(s) for the author(s) of this article can be found under https://doi.org/10.1002/lpor.202200325

DOI: 10.1002/lpor.202200325

operations such as polarization filtering, conversion, and beam splitting.[14] These devices show high efficiency but generally require processing precision, and is difficult to control other optical parameters while performing polarization-related functions. Complex polarization processing even requires multiple devices to be cascaded at the same time.[16,17] On the other hand, the generation of vector beams is more difficult. At first, the researchers used the mode selection in the laser cavity or the superposition of fundamental mode to generate the vector field.[18] This approach usually produces only a single type of vector beam and show limited energy efficiency. Later, devices such as polarization converters and space-variant subwavelength gratings were used.[19,20] The generation of vector light fields can also be achieved by the combination of spiral phase plates and wave plates.[21] In recent years, modern optoelectronic components such as spatial light modulators (SLM) and digital micromirror arrays (DMD) have been used more, which can generate different vector light fields in real time.[22–24] However, these schemes are almost limited in modulation efficiency, system volume and functional integration. With the continuous development of meta-optics,[25–27] metasurface-based polarization optics offer new possibilities for polarization manipulation.[28–30] The special symmetries of meta-atoms can induce differentiated electromagnetic responses of orthogonally polarized components, which in turn manipulate polarization and other parameters simultaneously.[31] For example, in addition to waveplates and polarizers, anisotropic metasurfaces of metals or dielectrics have achieved independent phase control of orthogonal linearly and circularly polarized waves,[32] and destructive or constructive interference of the two meta-atoms show amplitude control of arbitrary orthogonal components.[33,34] In addition, chiral metasurfaces with geometric phase have performed linear and nonlinear chiral wavefront control, and the simultaneous manipulation of multiple electromagnetic parameters.[35] In addition, metasurface-based vector beam generations have also been widely reported, the most important of which is the coherent superposition of orthogonal circularly polarized waves.[36]

Vector light fields have a wide range of applications in optical storage, laser processing, and optical micro-manipulation.[37] More polarization components and spatially varying dimensions in vector fields mean more control degrees of freedom and application functions. Initially, the generation and manipulation of vector fields focused on two-dimensional polarization distributions in a plane, including conventional schemes and meta-optics. In recent years, the three-dimensional design of vector light fields based on digital optical systems has been widely reported, which produces different vector distributions at different positions in the propagation direction.[38] For example, implementing independent vector beam generation in multiple focal planes,[39] and a non-iterative focal field shaping can generate vector beams with specific three-dimensional trajectories.[40] It is worth mentioning that different non-diffracting Bessel beams can be superimposed to produce cylindrical vector beams that continuously change along the propagation direction, which originate from the gradient phase difference between the orthogonal circularly polarized components.[41,42] These solutions based on digital optical systems generally require the construction of complex optical paths, such as spatial filtering modules based on 4f systems. Although the optical path can be appropriately simplified by means of split-screen multiplexing, the entire system still needs to occupy a large space.[40] Meta-optics can greatly reduce the volume of the system, and a single device realizes both the phase control of orthogonal polarization components and the superposition of beams.[43–47] However, the three-dimensional vector field generation based on Bessel beams has limited energy utilization, and only the manipulation of the radial (transverse) electric field component has been reported so far, and it is difficult to consider the axial(longitudinal) component.

In this paper, we propose a new scheme for manipulating the vector light field along the propagation direction, which can simultaneously control the axial and radial electric field components, which is demonstrated in the terahertz band. Coherent superposition of orthogonal circularly polarized vortex beams with opposite topological charges is obtained by using a metalens with a long focal depth, and the continuous variation of the radial electric field component in the transmission direction is realized by controlling their axial phase difference. Based on spin-orbit coupling effect of the focused circularly polarized light field, the axial electric field component also significant change along propagation direction in the form of orbital angular momentum (OAM) superposition state. Additionally, we achieve independent control of 3D vector light fields within different planes using a metalens with multiple focal points. This scheme based on a single device for simultaneously controlling the three electric field components of the vector fields in three spatial dimensions effectively expands the manipulation capability of the meta-devices for the vector electromagnetic field.

2. Metasurface Implementation

We wish to demonstrate two typical capabilities as a validation of our scheme, namely continuously varying vector field generation along the propagation direction and independent control of polarization distributions in multiple focal planes. As shown in **Figure 1**a, we use an all-silicon metasurface to achieve the above functions in terahertz band. By changing the structural size and spatial orientation of the meta-atoms, we perform independent phase design for the orthogonal circularly polarized waves (left- and right-handed circularly polarized, LCP and RCP), and then introduce a phase difference that varies along the transmission direction. Figure 1b shows the three-dimensional vector field manipulation of the proposed scheme. Three electric field components can be controlled simultaneously by long focal depth or multi-plane focusing, where the change of longitudinal component (Ez) originates from the spin–orbit coupling effect. The phase difference between the orthogonal circularly polarized components can be introduced in two ways, namely the propagation phase accumulated along the path and the initial phase of each focus, as shown in Figure 1c,d. The former can be considered as continuously changing, the latter takes values independently at different positions, and these phase differences correspond to three-dimensional vector fields with different polarization distributions. It is worth mentioning that beams show rotation effects in the direction of propagation have been reported for many years.[48,49] But these reports can be attributed to phase-based complex amplitude control and the polarization distributions are not considered, which mainly include the ways

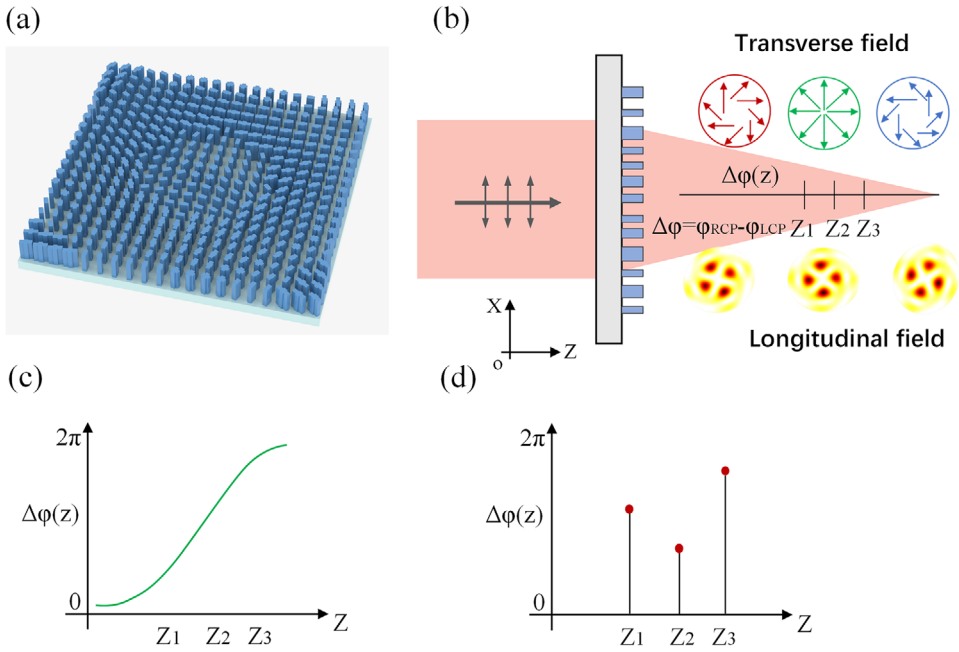

Figure 1. 3D vector beam generation based on metasurface. a) Schematic diagram of the all-silicon metasurface. b) Manipulation of transverse and longitudinal electric field components with a metalens. c) Continuously varying and d) discrete valued phase differences.

of Gouy phase or coherent superposition of double beams (with extra phase difference).

Firstly, we need to use the metasurface for independent phase control of the orthogonal circularly polarized components. Assume that the linearly polarized basis transmission matrix of the anisotropic meta-atom is

$$T = \begin{bmatrix} t_{xx} & 0 \\ 0 & t_{yy} \end{bmatrix} \tag{1}$$

where t_{xx} and t_{yy} are the transmission coefficients of the x- and y-polarized waves, respectively. After in-plane rotation of the meta-atom by an angle of θ, the phase relationship between the circularly cross-polarized components and the desired linearly polarized component is

$$\begin{aligned} \theta &= (\varphi_{RCP} - \varphi_{LCP})/4 \\ \varphi_{xx} &= (\varphi_{RCP} + \varphi_{LCP})/2 \\ \varphi_{yy} &= (\varphi_{RCP} + \varphi_{LCP})/2 - \pi \end{aligned} \tag{2}$$

A complete derivation process can be seen in the Supporting Information (part 1).

On the other hand, a vector beam with a vortex-type polarization distribution in cross-section can be represented by the Jones vector as

$$\mathbf{E}(r,\theta) = A(r) \begin{bmatrix} \cos(p\theta + \theta_0) \\ sin(p\theta + \theta_0) \end{bmatrix} \tag{3}$$

where A(r) is the complex amplitude, p is the topological charge of polarization, and θ_0 is the initial polarization angle. The vector beam can be obtained by coherent superposition of orthogonal circularly polarized vortex beams, assuming that the phase difference between them is $\Delta\varphi$, then

$$\frac{1}{2}e^{il\theta+\Delta\varphi}\begin{bmatrix}1\\-i\end{bmatrix} + \frac{1}{2}e^{-il\theta}\begin{bmatrix}1\\i\end{bmatrix} = e^{\frac{1}{2}i\Delta\varphi}\begin{bmatrix}\cos(l\theta+\frac{1}{2}\Delta\varphi)\\ sin(l\theta+\frac{1}{2}\Delta\varphi)\end{bmatrix} \tag{4}$$

It means that the initial polarization angle θ_0 of the generated vector beam is determined by $\Delta\varphi$. If $\Delta\varphi$ varies along the transmission direction, then

$$\theta_0(z) = \frac{1}{2}\Delta\phi(z) \tag{5}$$

3. Results and Discussion

To achieve the above functions, we designed two metasurfaces to show vector beam generation with continuous variation along the propagation direction and independent control of the polarization states in multiple focal planes, respectively (sample 1 and sample 2). The meta-atoms of both samples are made of highly resistive silicon. **Figure 2** shows the simulation results of sample 1. We use the time-domain solver of the commercial software to perform structural parameter sweeps of the meta-atoms, as shown in Figure 2a. Among them, the period is $P = 140$ μm, the thickness of the substrate is 300 μm, the column height is $H = 200$ μm, the rectangle width is $W = 40$ μm, and the lengths in the two directions are Lx and Ly, respectively. The dielectric constant of silicon is set in the simulation process as 11.9 without optical loss. We obtained the transmission amplitude and phase values for x and y polarization components under different dimensions, the detailed simulation settings and results are in the Supporting Information (part 2).

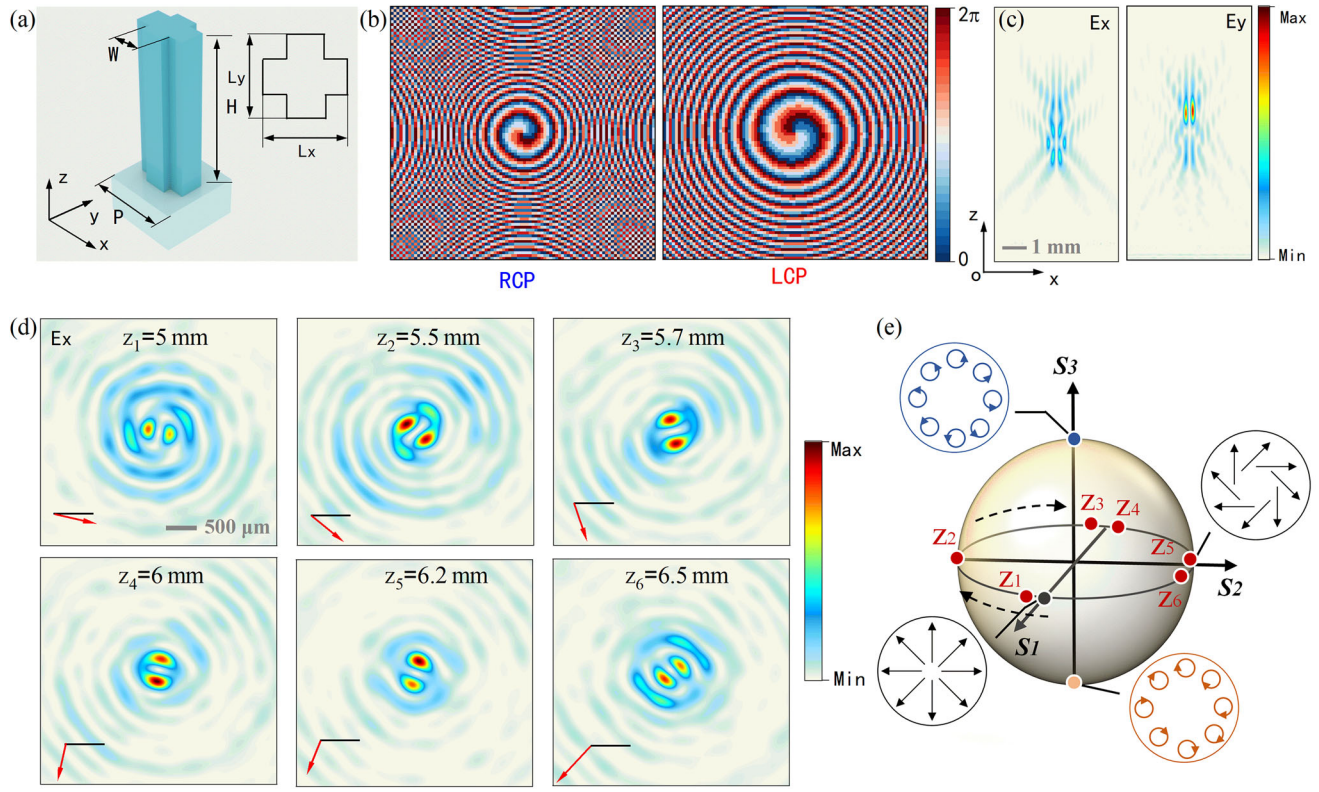

Figure 2. Generation of a vector beam that varies continuously along the propagation direction via a metasurface. a) Structural parameters of the meta-atoms. b) Design phases of LCP and RCP components. c) Longitudinal distributions of *x* and *y* polarization components in the transmitted vector field. d) Transverse distributions of the *x* component at different *z* coordinates. e) The evolution of the vector field on a higher-order Poincaré sphere.

In order to obtain the required axial continuously changing phase difference $\Delta\varphi(z)$, and to realize the manipulation of the three electric field components at the same time, we choose the focusing phase design with a long focal depth, and assign different focal lengths and positions to the left and right circular polarization components. The phase distributions of the two channels are[48]:

$$\varphi(r,\theta)_{\mathrm{RCP}} = k \cdot r^2/(f_1 + (\Delta f_1 \cdot r^2/R^2))/2 + l\theta$$
$$\varphi(r,\theta)_{\mathrm{LCP}} = k \cdot r^2/(f_2 + (\Delta f_2 \cdot r^2/R^2))/2 - l\theta \quad (6)$$

where k is the wave vector in free-space, R is radius of the metasurface, f_1 and Δf_1 are the designed focal points and length, respectively, l is the phase topological charge. Let $l_{\mathrm{R}} = 1$, $l_{\mathrm{L}} = -1$, $f_1 = 6000\ \mu$m, $\Delta f_1 = 1500\ \mu$m, $f_2 = 4000\ \mu$m, $\Delta f_2 = 2000\ \mu$m. The mean numerical aperture can be considered as $\mathrm{NA} = \sin[\mathrm{atan}(R \times 2/(f_1 + f_2))] = 0.783$. The obtained design phases of LCP and RCP waves are shown in Figure 2b, where the number of the units is 90 × 90. Using the full-wave simulation method, we obtained the three-dimensional transmitted light field when the *x*-polarized plane wave is incident. The electric field distribution of the *x*- and *y*-polarized components in the xoz plane are shown in Figure 2c, where the operating frequency is 1 THz. It can be found that the focal lengths of the *x* and *y* polarization components are significantly elongated. To further observe the change of the vector beam along the propagation direction, we selected 6 different positions to show the electric field of the transverse component (Ex, Ey), as shown in Figure 2d. The red arrows represent the orientation of the intensity, and the solid black line serves as the reference. Obviously, as the distance between the observation point and the lens gradually increases, the intensity orientation of Ex rotates, which means that the polarization distributions of the three-dimensional vector light field is gradually changing. This is due to the fact that the metalens we designed have different focal lengths and depths for the RCP and LCP components, that is, the two vortices will accumulate a phase difference related to the z-coordinate along different paths during the propagation process. A more intuitive representation of the vector field evolution is the higher-order Poincaré sphere, as shown in Figure 2e, where the topological charge of polarization is 1. We put the vector polarization states of the six positions in Figure 2d in the Poincaré sphere. Within the propagation distance from z_1 to z_6, the phase difference covers a range of more than $3\pi/2$, which means that the change of the initial polarization angle θ_0 exceeds $3\pi/4$ within the distance.

We use ICP (Inductively Coupled Plasma) etching technology to process the sample based on commercial high-resistance silicon wafers with a thickness of 500 μm, and the prepared sample 1 is in **Figure 3**. For the detailed preparation process, see Supporting Information (part 3). Figure 3a shows a SEM (scanning electron microscope) photograph of the sample, where the white scale bar is 100 μm. We measured the transmitted terahertz beam of sample 1 using the 2D electro-optic sampling system in

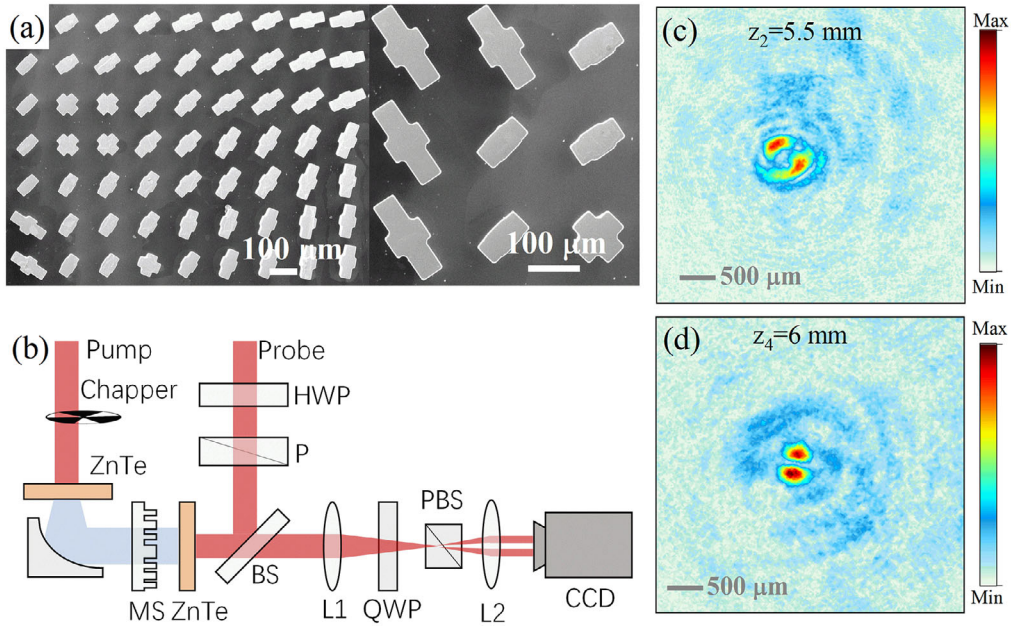

Figure 3. Experimental results of the sample 1. a) Local scanning electron microscope (SEM) photo of sample 1, the scale bars are 100 μm. b) The optical path of the THz time-domain system. c,d) Intensities of the *x* component at different *z* coordinates.

Figure 3b, which is supported by an amplified femtosecond laser system (Spectra-Physics, USA) with pump and probe beams (center wavelengths of 800 nm, spot diameter of 8 mm, repetition rate of 1 kHz). Two ZnTe crystals are used to radiate and detect the terahertz signals, respectively, and the sample (MS) was placed between them. The femtosecond laser signal modulated by the terahertz electric field is transmitted to the CCD (charge coupled device) camera through a 4f system, and a quarter-wave plate (QWP) and a polarization beam splitter (PBS) are used to achieve balanced detection. Since the frequency of the sample is not at the optimal frequency of the system, and the long focal length leads to the weakening of the signal strength, we have only measured the co-polarized components at the positions of z_2 and z_3, which show relatively large signal to noise ratio (SNR). The measured results are shown in Figure 3c,d, which are in good agreement with the simulation results in Figure 2d.

In the previous section, we have achieved continuous variation of the terahertz vector field in the direction of transmission. Here we will show independent control of the polarization distributions of the field in multiple focal planes, which means that $\Delta\varphi$ will be designed as different values at several discrete z-coordinates. Taking the vertical double-point focusing as an example, the designed phase distributions of two orthogonal circularly polarized components in the metasurface are

$$\begin{aligned}\varphi(r,\theta)_{\mathrm{LCP}} &= \arg\left(e^{k\cdot\sqrt{r^2+f_3^2}+l\theta+\Delta\varphi_1}+e^{k\cdot\sqrt{r^2+f_4^2}+l\theta+\Delta\varphi_2}\right)\\ \varphi(r,\theta)_{\mathrm{RCP}} &= \arg\left(e^{k\cdot\sqrt{r^2+f_3^2}-l\theta}+e^{k\cdot\sqrt{r^2+f_4^2}-l\theta}\right)\end{aligned} \tag{7}$$

where $f_3 = 5$ mm, $f_4 = 8.5$ mm, the initial phase differences corresponding to the two focal planes are $\Delta\varphi_1 = \pi/2$, $\Delta\varphi_2 = -\pi/2$. Different from sample 1, here the phase topological charge of RCP and LCP waves are $l_R = -1$, and $l_L = +1$.

We designed and experimentally verified sample 2 using a similar method to sample 1, and the SEM photo is shown in **Figure 4**a. Figure 4b shows the design phase of the LCP and RCP components calculated by formula (7), the two channels show opposite phase change directions. We set the *x* plane wave incidence and simulated the transmission field of sample 2. The electric field intensities of the *x*-component in transmitted terahertz beam on two planes ($z_1 = 4.7$ mm, $z_2 = 8.1$ mm) are shown in Figure 4c,d, where the two radial vector fields show opposite polarization distributions. The measured results are shown in Figure 4e,f, which are consistent with the simulations. To further confirm the polarization distribution of the transmitted field, we show the terahertz vector field distributions of the two planes in Figure 4g,h, where the z-direction electric field is very weak.

In addition to the transverse electric field components, the proposed metasurfaces also appear to be very powerful in manipulating the longitudinal electric field component (Ez) in the propagation direction. It is well known that a tightly focused beam will produce an axial (longitudinal) electric field component. More interestingly, the focusing of a circularly polarized beam will exhibit spin–orbit coupling effects in the Ez component,[46] as far as we know, manipulating the axial electric field component in the propagation path has not almost been reported before. Here we first study the sample 1. In the previous section, we have explained that the design topological charges of the two circularly polarized components in sample 1 are $l_L = -1$, $l_R = +1$, respectively. According to the spin–orbit coupling principle of focused light fields[49]:

$$l_{\mathrm{Longitudinal}} = l_{\mathrm{Transverse}} + \sigma \tag{8}$$

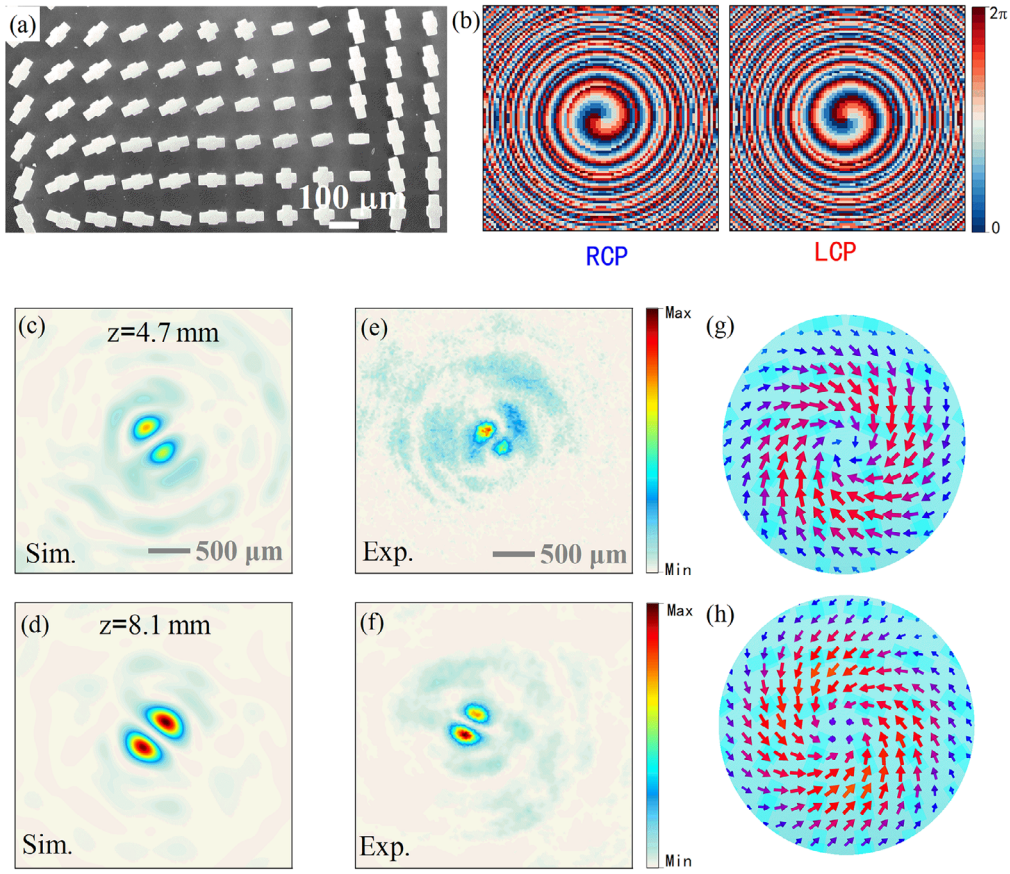

Figure 4. Generation of the vector beams with independently controlled polarization distributions in two focal planes using metasurface. a) SEM image of sample 2, the scale bar is 100 μm. b) Phase design of multi-point focusing for LCP and RCP wave. c–f) Simulated and measured results of the Ex component in the two focal planes. g,h) The three-dimensional electric field distribution of the vector field in the two focal planes.

where $\sigma = \pm 1$ is the spin angular momentum, the topological charges of the longitudinal electric field components induced by the two circularly polarized components will be 2 and −2, respectively. This means that we will observe a gradually changing longitudinal electric field component as OAM superposition state in the propagation direction.

To verify the above analysis, we further simulated sample 1 to obtain the transmitted terahertz fields when the circularly and linearly polarized plane waves were incident. **Figure 5**a–f shows the Ez components in the transmitted field, including transverse and longitudinal slices, under the incidence of RCP and LCP waves, respectively. From the phase distributions in Figure 5b,e, it can be seen that the phase topological charges of Ez component caused by the LCP and RCP components are −2 and 2, respectively. The normalized intensity relationship of the three electric field components in the transmission vector field is shown in Figure 5g,h, and the intensity of Ez is about 1/5 of the radial field component. The generation efficiency of the longitudinal component can be improved by adjusting the numerical aperture of the lens,[50,51] longitudinal electric field generation of our metasurfaces with different focal lengths can be seen in the Supporting Information (Figure S4, Supporting Information). When the incident wave is linearly polarized, it can be considered as the simultaneous incidence of two circularly polarized components. Figure 5i–n shows the longitudinal field components induced by the linearly polarized incident wave, which appears as a second-order vortex interference field, and the intensity distributions change along the propagation direction. This is also due to the phase difference in the orthogonal circularly polarized waves. The Ez component of sample 2 is similar to that of sample 1, which can be seen in Supporting Information (part 5).

4. Conclusion

In summary, we demonstrate a new scheme for 3D vector light field regulation based on all-dielectric metasurfaces. By introducing the phase difference accumulated by the propagation path as well as the initial difference between the orthogonal circularly polarized components, the effective control of the polarization distribution of the vector field in the propagation direction is achieved. We designed two samples in the terahertz band for experimental verification, using a long focal depth and a longitudinal multifocal metalens to demonstrate the continuous variation and multi-plane independent control of the vector light field on the propagation path, respectively. It is worth mentioning that our scheme can not only design the polarization distribution of the transverse electric field components, but also effectively generate and control the wave propagation of the longitudinal

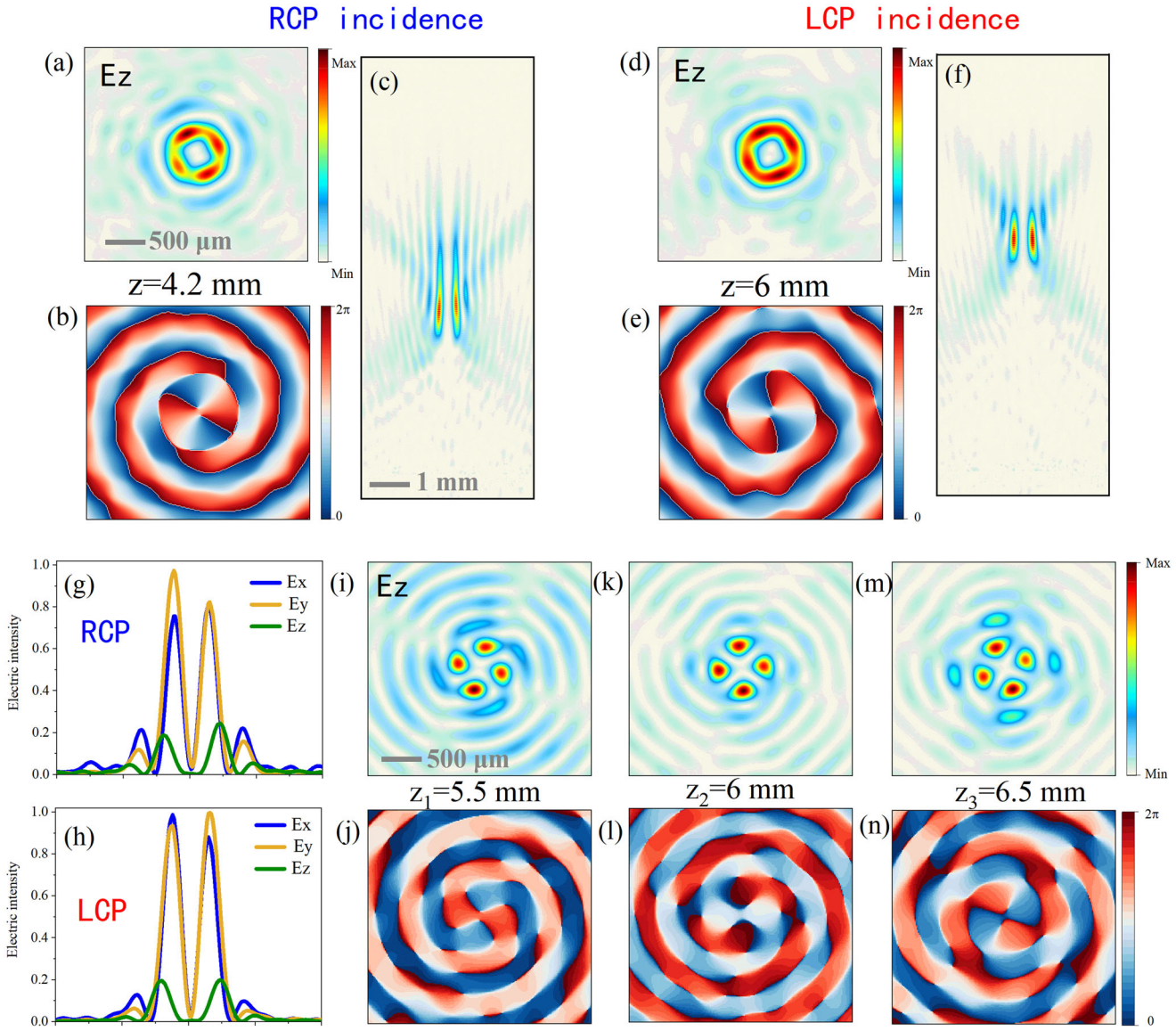

Figure 5. Longitudinal electric field components of sample 1. a–f) Intensity and phase distributions of Ez components with LCP or RCP wave incidence. g,h) Intensity comparison of three electric field components. i–n) The intensity and phase distributions of the Ez component, when the *x*-polarized wave is incident.

component. This scheme demonstrates the generation of three-dimensional vector field with three-dimensional spatial distribution changes using a single metasurface, which provides a new idea for the generation and manipulation of vector light fields based on metasurfaces.

Supporting Information

Supporting Information is available from the Wiley Online Library or from the author.

Acknowledgements

J.L., J.L., and Z.Y. contributed equally to this work. This work was supported by the National Key Research and Development Program of China (Nos. 2021YFB2800703 and 2017YFA0700202); National Natural Science Foundation of China (Nos.61675147, 61735010, and 91838301).

Conflict of Interest

The authors declare no conflict of interest.

Data Availability Statement

The data that support the findings of this study are available from the corresponding author upon reasonable request.

Keywords

longitudinal fields, metasurfaces, terahertz, vector fields

Received: May 5, 2022
Revised: July 15, 2022
Published online:

[1] J. Leach, J. Courtial, K. Skeldon, S. M. Barnett, S. Franke-Arnold, M. J. Padgett, *Phys. Rev. Lett.* **2004**, *92*, 4.
[2] D. F. Gordon, B. Hafizi, A. Ting, *Opt. Lett.* **2009**, *34*, 3280.
[3] M. Schäferling, *Chiral Nanophotonics*, Springer International Publishing, Cham **2017**.
[4] J. Lu, Y. Xue, K. Bernardino, N. N. Zhang, W. R. Gomes, N. S. Ramesar, S. Liu, Z. Hu, T. Sun, A. F. de Moura, N. A. Kotov, K. Liu, *Science* **2021**, *371*, 1368.
[5] K. Y. Bliokh, F. J. Rodríguez-Fortuño, F. Nori, A. V. Zayats, *Nat. Photonics* **2015**, *9*, 796.
[6] X. Ling, X. Zhou, K. Huang, Y. Liu, C. W. Qiu, H. Luo, S. Wen, *Rep. Prog. Phys.* **2017**, *80*, 066401.
[7] J. S. Eismann, L. H. Nicholls, D. J. Roth, M. A. Alonso, P. Banzer, F. J. Rodríguez-Fortuño, A. V. Zayats, F. Nori, K. Y. Bliokh, *Nat. Photonics* **2021**, *15*, 156.
[8] A. B. Khanikaev, G. Shvets, *Nat. Photonics* **2017**, *11*, 763.
[9] Y. Wu, C. Li, X. Hu, Y. Ao, Y. Zhao, Q. Gong, *Adv. Opt. Mater.* **2017**, *5*, 1700357.
[10] F. Gao, H. Xue, Z. Yang, K. Lai, Y. Yu, X. Lin, Y. Chong, G. Shvets, B. Zhang, *Nat. Phys.* **2018**, *14*, 140.
[11] Z. Wang, C. Xie, X. Ren, *Opt. Express* **2009**, *17*, 7993.
[12] G. Dolgos, J. V. Martins, *Opt. Express* **2014**, *22*, 21972.
[13] L. Xu, Y. Feng, D. Yu, Z. Zheng, X. Chen, W. Hong, *Adv. Mater. Technol.* **2020**, *5*, 2000373.
[14] D. Goldstein, *Polarized Light*, 2nd ed., Marcel Dekker, New York **2003**.
[15] A. Forbes, M. de Oliveira, M. R. Dennis, *Nat. Photonics* **2021**, *15*, 253.
[16] S. Fu, C. Guo, G. Liu, Y. Li, H. Yin, Z. Li, Z. Chen, *Phys. Rev. Lett.* **2019**, *123*, 243904.
[17] W. Zhu, H. Zheng, Y. Zhong, J. Yu, Z. Chen, *Phys. Rev. Lett.* **2021**, *126*, 83901.
[18] V. G. Niziev, R. S. Chang, A. V. Nesterov, *Appl. Opt.* **2006**, *45*, 8393.
[19] G. Machavariani, Y. Lumer, I. Moshe, A. Meir, S. Jackel, *Opt. Commun.* **2008**, *281*, 732.
[20] Z. Bomzon, G. Biener, V. Kleiner, E. Hasman, *Opt. Lett.* **2002**, *27*, 1141.
[21] S. M. Li, S. X. Qian, L. J. Kong, Z. C. Ren, Y. Li, C. Tu, H. T. Wang, *EPL* **2014**, *105*, 64006.
[22] S. Liu, S. Qi, Y. Zhang, P. Li, D. Wu, L. Han, J. Zhao, *Photonics Res.* **2018**, *6*, 228.
[23] A. J. Macfaden, T. D. Wilkinson, *J. Opt. Soc. Am. A* **2017**, *34*, 161.
[24] J. Chen, Y. Wang, C. Wan, K. Lu, Y. Liu, Q. Zhan, *Opt. Commun.* **2021**, *495*, 127112.
[25] H. Duan, Y. Hu, X. Wang, X. Luo, X. Ou, L. Li, Y. Chen, P. Yang, S. Wang, *Nanophotonics* **2020**, *9*, 3755.
[26] C. Gong, Z. Pan, M. I. Dedo, J. Sun, L. Wang, Z. Guo, *Results Phys.* **2021**, *30*, 104829.
[27] W. Wang, Q. Yang, S. He, Y. Shi, X. Liu, J. Sun, K. Guo, L. Wang, Z. Guo, *Opt. Express* **2021**, *29*, 43270.
[28] H. Zhou, L. Chen, F. Shen, K. Guo, Z. Guo, *Phys. Rev. Appl.* **2019**, *11*, 024066.
[29] S. Chen, W. Liu, Z. Li, H. Cheng, J. Tian, *Metamaterials - Devices Applications*, IntechOpen, London **2017**.
[30] F. Ding, B. Chang, Q. Wei, L. Huang, X. Guan, S. I. Bozhevolnyi, *Laser Photonics Rev.* **2020**, *14*, 2000116.
[31] S. Chen, Z. Li, Y. Zhang, H. Cheng, J. Tian, *Adv. Opt. Mater.* **2018**, *6*, 1800104.
[32] A. Arbabi, Y. Horie, M. Bagheri, A. Faraon, *Nat. Nanotechnol.* **2015**, *10*, 937.
[33] F. Zhang, M. Pu, X. Li, P. Gao, X. Ma, J. Luo, H. Yu, X. Luo, *Adv. Funct. Mater.* **2017**, *27*, 1704295.
[34] Q. Fan, M. Liu, C. Zhang, W. Zhu, Y. Wang, P. Lin, F. Yan, L. Chen, H. J. Lezec, Y. Lu, A. Agrawal, T. Xu, *Phys. Rev. Lett.* **2020**, *125*, 267402.
[35] L. Kang, S. P. Rodrigues, M. Taghinejad, S. Lan, K. T. Lee, Y. Liu, D. H. Werner, A. Urbas, W. Cai, *Nano Lett.* **2017**, *17*, 7102.
[36] J. Han, Y. Intaravanne, A. Ma, R. Wang, S. Li, Z. Li, S. Chen, J. Li, X. Chen, *Laser Photonics Rev.* **2020**, *14*, 2000146.
[37] C. Rosales-Guzmán, B. Ndagano, A. Forbes, *J. Opt.* **2018**, *20*, 123001.
[38] E. Otte, C. Rosales-Guzmán, B. Ndagano, C. Denz, A. Forbes, *Light: Sci. Appl.* **2018**, *7*, 18009.
[39] H. Chen, Z. Zheng, B.-F. Zhang, J. Ding, H.-T. Wang, *Opt. Lett.* **2010**, *35*, 2825.
[40] J. A. Rodrigo, T. Alieva, E. Abramochkin, I. Castro, *Opt. Express* **2013**, *21*, 20544.
[41] R. P. Chen, Z. Chen, Y. Gao, J. Ding, S. He, *Laser Photonics Rev.* **2017**, *11*, 1700165.
[42] S. Fu, S. Zhang, C. Gao, *Sci. Rep.* **2016**, *6*, 1704295.
[43] C. Chang, Y. Gao, J. Xia, S. Nie, J. Ding, *Opt. Lett.* **2017**, *42*, 3884.
[44] A. H. Dorrah, M. Tamagnone, N. A. Rubin, A. Zaidi, F. Capasso, *Nanophotonics* **2021**, *11*, 713.
[45] A. H. Dorrah, N. A. Rubin, A. Zaidi, M. Tamagnone, F. Capasso, *Nat. Photonics* **2021**, *15*, 287.
[46] A. H. Dorrah, N. A. Rubin, M. Tamagnone, A. Zaidi, F. Capasso, *Nat. Commun.* **2021**, *12*, 6249.
[47] F. Zhang, M. B. Pu, Y. H. Guo, X. L. Ma, X. Li, P. Gao, X. G. Luo, *Sci. China: Phys., Mech. Astron.* **2022**, *65*, 254211.
[48] X. F. Zang, W. W. Xu, M. Gu, B. S. Yao, L. Chen, Y. Peng, J. Y. Xie, A. V. Balakin, A. P. Shkurinov, Y. M. Zhu, S. L. Zhuang, *Adv. Opt. Mater.* **2020**, *8*, 1901342.
[49] Y. Y. Schechner, *Phys. Rev. E* **1996**, *54*, R50.
[50] P. Pääkkönen, J. Lautanen, M. Honkanen, M. Kuittinen, J. Turunen, S. N. Khonina, V. V. Kotlyar, V. A. Soifer, A. T. Friberg, *J. Mod. Opt.* **1998**, *45*, 2355.
[51] Y. Zhao, J. S. Edgar, G. D. M. Jeffries, D. McGloin, D. T. Chiu, *Phys. Rev. Lett.* **2007**, *99*, 15.

